High performance bi-functional quantum cascade laser and detector

Benedikt Schwarz, Daniela Ristanic, Peter Reininger, Tobias Zederbauer, Donald MacFarland, Hermann Detz, Aaron Maxwell Andrews, Werner Schrenk, and Gottfried Strasser

Citation: Applied Physics Letters **107**, 071104 (2015); doi: 10.1063/1.4927851
View online: http://dx.doi.org/10.1063/1.4927851
View Table of Contents: http://scitation.aip.org/content/aip/journal/apl/107/7?ver=pdfcov
Published by the AIP Publishing

High performance bi-functional quantum cascade laser and detector

Benedikt Schwarz,[1,a)] Daniela Ristanic,[1] Peter Reininger,[1] Tobias Zederbauer,[1] Donald MacFarland,[1] Hermann Detz,[1,2] Aaron Maxwell Andrews,[1] Werner Schrenk,[1] and Gottfried Strasser[1]

[1]*Institute for Solid State Electronics and Center for Micro- and Nanostructures, TU Wien, Floragasse 7, 1040 Vienna, Austria*

[2]*Austrian Academy of Sciences, Dr. Ignaz Seipel-Platz 2, 1010 Vienna, Austria*

(Received 6 June 2015; accepted 23 July 2015; published online 17 August 2015)

An improved bi-functional quantum cascade laser and detector emitting and detecting around 6.8 μm is demonstrated. The design allows a significantly higher laser performance, showing that bi-functional designs can achieve a comparable pulsed performance to conventional quantum cascade lasers. In particular, the device has a threshold current density of 3 kA/cm^2, an output power of 0.47 W, and a total wall-plug efficiency of 4.5% in pulsed mode. Optimized electron extraction and the prevention of thermal backfilling allow higher duty cycles, operation up to 10%, with 15 mW average output power at room temperature without optimization of the laser cavity or coatings. At zero bias, the device has a responsivity of around 40 mA/W and a noise equivalent power of 80 pW/$\sqrt{\text{Hz}}$ at room temperature, which in on-chip configuration outperforms conventional uncooled discrete detectors.
[http://dx.doi.org/10.1063/1.4927851]

Quantum cascade lasers (QCLs) have proven to be an extremely useful and versatile source of mid-infrared and THz radiation. Since their first demonstration by Faist *et al.*,[1] mid-infrared QCL has been shown to emit watt level continuous wave output power at room temperature,[2] achieve wall-plug efficiencies of up to 50%,[3,4] emit single mode using distributed feedback gratings,[5] or emit over a broadband spectral range using multiple stacks of different active regions.[6,7] Nowadays, QCLs are used in many sensing and spectroscopic applications ranging from environmental monitoring, e.g., for trace gas monitoring,[8] to life sciences, e.g., for blood serum analysis.[9] Compact sensing systems have been successfully realized using QCLs together with MCT detectors in direct and cavity enhanced absorption spectroscopy setups, enabling up to parts per billion detection.[10] Even more compact sensing systems have been developed using quartz enhanced photo-acoustic techniques, where substances are detected via the resonant excitation of sound waves through the thermal expansion of gases.[11] Following up on these concepts, the next logical step is the development of chip-scale sensing devices, requiring the integration of light sources, detectors, and interaction regions on a single chip. Chemicals in liquid phase can be directly probed on stripe waveguides[12,13] or Mach-Zehnder interferometers,[14] but chip-scale gas sensors require more advanced techniques to enhance the interaction, e.g., microdisk/ring resonators[15] or Mach-Zehnder interferometers with sensitive polymer layers.[16]

Quantum cascade detectors (QCDs)[17,18] originate from photovoltaic quantum well photodetectors[19] and photocurrent measurements of QCLs.[20] In QCDs, absorbed electrons are extracted through a staircase of subbands that provides a preferential direction for the carriers through an effective built-in field and allows zero bias operation. Due to the short carrier lifetimes, QCDs are fast, have high saturation intensities, and thus, they are an ideal counterpart for QCLs with high peak power levels.

Going one step further, the QCL and QCD functionality can be combined within the very same epilayer material.[21] Such bi-functional quantum cascade lasers and detectors (QCLDs) enable the generation and detection of mid-infrared radiation of the same wavelength on the same chip, allowing for monolithic integration. Based on QCLDs, a monolithically integrated sensor prototype capable of detecting concentration fractions in a chemical solution has been realized.[22] Plasmonic waveguides were used to provide efficient coupling from the laser to the detector, as well as to provide a strong interaction with the environment through the evanescent character of the surface plasmon polaritons. The use of distributed feedback lasers and on-chip temperature monitoring allows a significant reduction in the minimum detectable concentration[23] and fabricated as an array of laser/waveguide/detector units such a sensor will provide selective detection of individual chemicals in complex mixtures. Recently, a QCLD working at 9.5 μm has been integrated together with germanium waveguides aiming for on-chip gas sensing.[24]

The main challenges in the design of QCLDs are the optimization of both operation modes while maintaining the spectral overlap between the laser emission and the photoresponse. This requirement limits the achievable performance of QCLDs compared to conventional QCLs. Our previous designs[21,22] showed room temperature operation for both the laser and the detector, but were limited to low duty-cycle operation, due to the large threshold current densities and low wall-plug efficiencies. High performance QCL designs are commonly based on resonant optical phonon extraction, where thin barriers are used to maximize the overlap with

[a)]Electronic mail: benedikt.schwarz@tuwien.ac.at

the extractor subbands and to provide a large energy separation in order to prevent thermal back filling of electrons from the injector to the lower laser subband. For bi-functional QCLD designs, this optimization cannot be fully exploited as the strong coupling of the lower laser subband and the extractor subbands would lead to a large wavelength-shift between the laser and the detector operation modes.[21] In our previous QCLD designs, wavelength matching was achieved by using broader barriers, with the drawback of a significantly reduced laser performance in terms of threshold current, efficiency, and output power. In this Letter, we demonstrate a refined design approach for QCLDs, showing that bi-functional operation can be achieved without a large performance drawback in both operation modes.

The banddiagram of the presented bi-functional active region for both operation modes is shown in Figure 1. Similar to the previous QCLDs, thicker barriers are used to achieve wavelength matching. Additionally, we use a slightly more diagonal transition, giving another knob to compensate the stark-shift introduced by the extraction levels. The thicker barriers lead to a more horizontal electron extraction through scattering assisted tunneling rather than

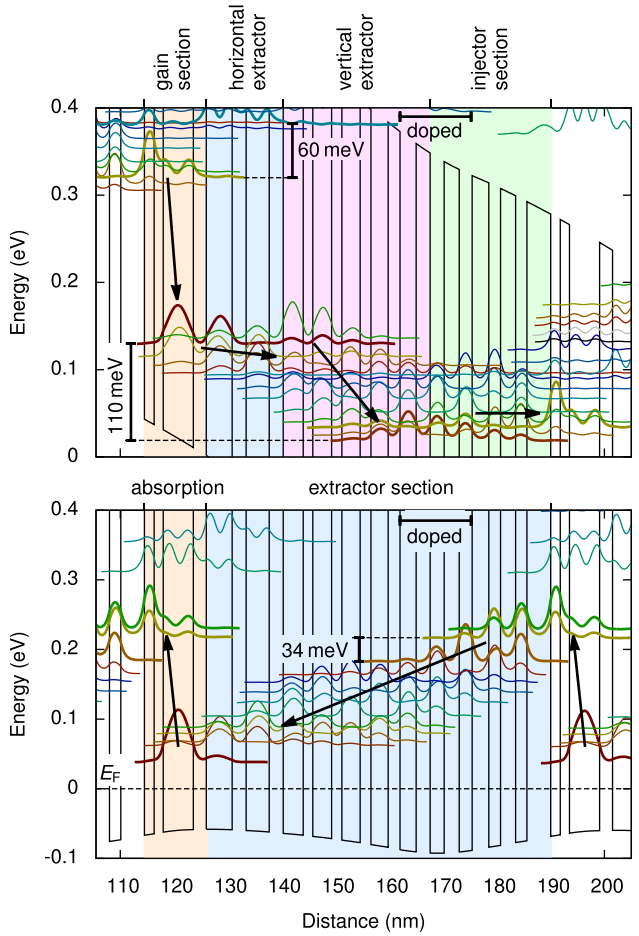

FIG. 1. Band diagram of the improved bi-functional QCLD for laser bias at the maximal wallplug efficiency (upper) and detector (zero) bias. The different logical sections are highlighted in color and the preferred electron transport direction is denoted with black arrows. The banddiagrams are obtained solving Schrödinger's equation self-consistently with Poisson's equation using the subband populations calculated by single particle Monte-Carlo transport.[25] The detector is in thermal equilibrium with the Fermi level denoted by the dashed line.

the usually used vertical extraction via an LO-phonon stair. For wavelength matching, it is sufficient that the first 2–3 barriers are thicker. The second extractor part is designed with thin barriers to vertically extract electrons and to prevent thermal backfilling via several strongly coupled subbands with high energy separation. The energy separation from the lowest injector subband and the lower laser subband is 90 meV at threshold and 110 meV at the peak of the wallplug efficiency. This design approach also gives a higher separation of the upper laser subband and its next upper subband (60 meV at peak WPE) as well as a minigap in the injector to reduce the electron escape probability to the continuum. As discussed in Ref. 21, the third part (injector section) has to be designed to provide sufficient electron injection into the upper subband at the laser bias as well as to provide efficient extraction from the upper subband to the injector subbands at the detector bias (zero bias). The energetically highest subband in the injector section has no function at QCL bias, but acts as detector extraction level at zero bias. As a negative drawback, this subband may introduce a small additional electron escape probability through the subbands above the upper laser subbands to the continuum. The slightly diagonal transition is also beneficial to optimize the electron extraction efficiency from the upper subband in detector operation.[26] For the device design, we used the efficient single particle Monte-Carlo transport simulator within the simulation framework VSP2, described more detailed in Ref. 25.

The structure was grown by molecular beam epitaxy from lattice-matched InGaAs/InAlAs on InP. The 35 periods of the active region are embedded in two low-doped InGaAs layers to increase the confinement. Specifically, designed contact super-lattice structures between the active region and the InGaAs layers enable efficient filling of the first lower detector subband, as well as efficient charge transport at detector and laser biases to prevent charge accumulations and series resistances. Care must be taken to prevent the contact superlattices from introducing resonant absorption loss through intersubband transitions. The layer structure starting from the InP substrate ($2 \times 10^{17}\,\mathrm{cm}^{-3}$) is as follows (for superlattices the InAlAs barriers are in bold): 550 nm InGaAs ($5 \times 10^{16}\,\mathrm{cm}^{-3}$); bottom contact super-lattice: **2.6**, 4.3, **2.6**, 4.3, **2.2**, 3.2, **2.0**, 3.4, **1.9**, 3.5, **1.8**, 3.7, **2.6**, 4.3, **2.6**, 4.8 nm with underlined layers n-doped with $5 \times 10^{17}\,\mathrm{cm}^{-3}$; 35 periods of the active region: **2.4**, 5.6, **1.7**, 1.8, **4.4**, 2.1, **2.8**, 2.2, **3.1**, 2.4, **2.8**, 2.6, **2.6**, 3.0, **2.2**, 3.2, **2.0**, 3.4, **1.9**, 3.5, **1.8**, 3.7, **2.6**, 4.3, **2.6**, 4.8 nm with underlined layers n-doped with $1.5 \times 10^{17}\,\mathrm{cm}^{-3}$; top contact super-lattice: **2.0**, 5.0, **2.0**, 6.0, **2.0**, 7.0, **2.0** nm n-doped with $1.5 \times 10^{17}\,\mathrm{cm}^{-3}$; 400 nm InGaAs ($5 \times 10^{16}\,\mathrm{cm}^{-3}$); 1200 nm and 800 nm InAlAs top cladding ($1 \times 10^{17}\,\mathrm{cm}^{-3}$ and $2 \times 10^{17}\,\mathrm{cm}^{-3}$); 350 nm InGaAs plasmon layer ($8 \times 10^{18}\,\mathrm{cm}^{-3}$). The 10 μm wide laser and detector ridges were fabricated by reactive ion etching of vertical sidewalls, followed by SiN insulation, Ti/Au contact deposition, rapid thermal annealing, and cleaving to 3 mm and 0.5 mm long devices for the laser and the detector, respectively. The devices were soldered epi-up with indium on a copper plate without substrate thinning.

The light, voltage, and total wall-plug efficiency versus current characteristic of the 3 mm long Fabry-Perot ridge

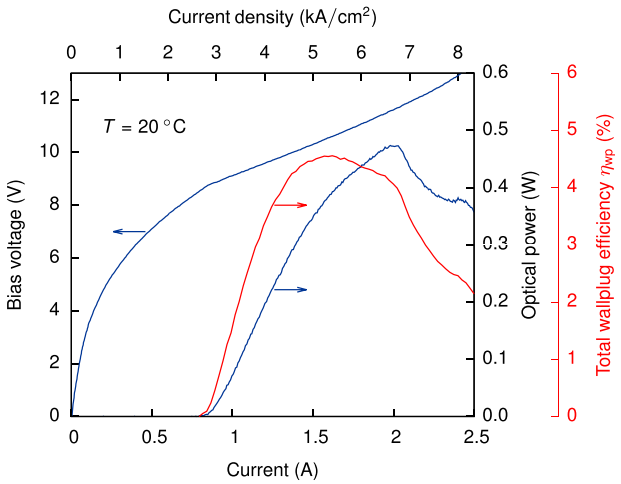

FIG. 2. Bias voltage, optical output power, and total wallplug efficiency in pulsed mode 100 ns at 10 kHz of the uncoated 10 μm wide and 3 mm long ridge. The total wallplug efficiency includes the optical power emitted from both facets.

laser is shown in Figure 2. Compared to our previous designs,[21,22] all characteristic parameters are improved by at least a factor of two. At room temperature, the threshold current density is reduced from 8 kA/cm^{-2} and 6 kA/cm^{-2} to 3 kA/cm^{-2}. The optical output power is increased from 40 mW and 200 mW to 470 mW. The laser has a total wallplug efficiency (considering both facets) of around 5%, which is a factor of two to three lower than for conventional high performance QCLs with comparable waveguide structures. Further improvements can be achieved by applying high- and anti-reflection coatings on the facets, as well as by using buried heterostructure waveguides with InP cladding to decrease the waveguide losses and increase the heat dissipation.[27]

Figure 3 shows the spectral overlap of the laser emission and the photoresponse. The presented detector has a peak responsivity of approximately 40 mA/W. In the on-chip configuration, direct end-fire coupling from a waveguide to a detector allows the use of a ridge waveguide geometry. As a general advantage of such integrated optical systems, the ridge detector allows high coupling and absorption

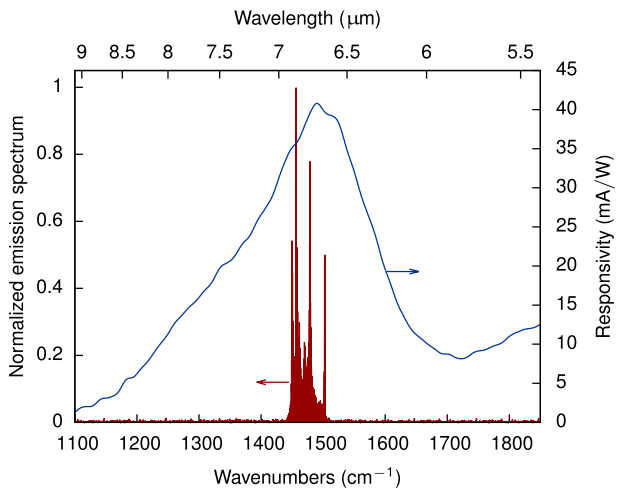

FIG. 3. Overlap of the emission spectrum and the spectral responsivity of the presented QCLD structure.

efficiencies with small absorption coefficients (reduced doping) and detector areas. As this is a huge benefit, the on-chip integrated QCLD ridge detector can outperform available discrete detectors at the same operation temperature. It has to be noted that this benefit is a general geometric property and would also apply for hybrid integrated MCT detectors that generally show a higher noise equivalent power (NEP), but lower saturation thresholds. The characterization was performed using an external source focused onto the detector ridge facet with a 10 cm focal length lens. The total power impinging on the detector was obtained by considering the beam-shape and the dimensions of the ridge facet. The device has a differential resistance of 1.6 kΩ around zero bias, which results in a Johnson/thermal noise limited NEP of 80 pW/$\sqrt{\text{Hz}}$ at the peak wavelength at room temperature.[28] For practical reasons, the detector was cleaved to 0.5 mm length, although anything longer than 50 μm does not increase the absorption efficiency significantly, but reduces the device resistance. For the on-chip sensor configuration, where the detector length is defined by optical lithography and dry etching, much shorter devices in the order of tens of micrometers can be used. A length of 15 μm would give the optimal Johnson noise limited NEP, while slightly longer devices around 50 μm give a higher responsivity and are favorable if the noise is limited by other sources.

For the signal-to-noise ratio of QCLD based sensors, one has to include all other noise sources, such as laser power fluctuations and temperature drift, as well as the particular device configuration. In the presented prototype sensor, the resolution is limited mainly by the emission power fluctuation of the laser; the noise of the detector is not as influential.[22] However, a reduced detector noise will be useful to improve the sensor resolution for devices with a longer absorption length or in the presence of high background absorptions. Furthermore, a higher device resistance allows a higher amplifier bandwidth or transimpedance gain.

We also tested the detector in the on-chip configuration with a small air gap between the laser and the detector. With a slightly shorter laser, we obtained a peak absolute photocurrent of 9 mA without observing detector saturation. It has to be noted that at such high optical power levels a low input impedance of the amplifier (transimpedance amplifier) or oscilloscope (50 Ω) is mandatory to maintain detector operation near zero bias. If not, the detector will be charged to a significant reverse bias (2–3 V), leading to a strong saturation effect. Due to the wavelength shift of the laser emission spectrum and the wavelength dependent coupling efficiency through the air gap, the on-chip detector shows a slightly different response (5%–10%) compared to an external broadband detector. The emission spectra of the laser at different currents are shown in Figure 4. The slightly diagonal transition leads to laser an emission spectrum which tunes with increasing bias. This feature may be utilized to gain information about the typically broad spectral features of chemicals in liquid phase without the need of an array of single mode lasers.

In conclusion, we presented an improved bi-functional quantum cascade laser/detector design with a comparable pulsed performance to conventional QCLs. The device has a significantly reduced threshold current density of 3 kA/cm^2

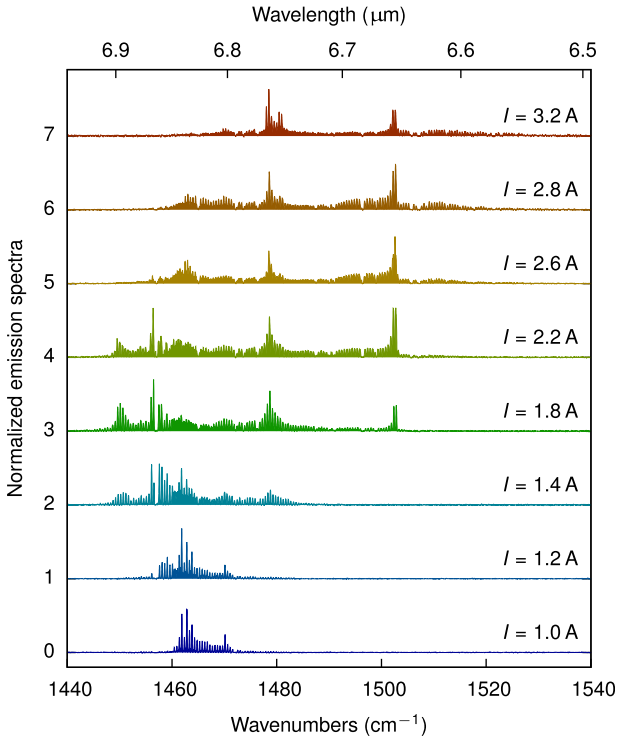

FIG. 4. Pulsed laser emission spectra with increasing current. The laser spectrum shifts to shorter wavelength, which might be utilized for on-chip sensor to obtain spectral information of the absorption features.

over previous bi-functional designs, emits 0.47 W peak power, and has a total wall-plug efficiency of 4.5%. The device can operate at high-duty cycles (10% with 100 ns pulses) with average output power of up to 15 mW at room temperature, without any thermal optimization of the cavity. On-chip sensing applications will greatly benefit from the lower current densities and higher duty cycle operation. In detector operation, the device has a responsivity of around 40 mA/W and in the on-chip configuration, it can outperform conventional discrete detectors in terms of noise equivalent power as well as saturation intensity.

This work was supported by the Austrian Science Funds (FWF) in the framework of the Doctoral School Building Solids for Function (Project W1243) and the project NextLite F4909-N23, as well as by the FP7 EU-project ICARUS (FP7-SEC-2011-285417). H.D. acknowledges funding through an APART Fellowship of the Austrian Academy of Sciences.

[1]J. Faist, F. Capasso, D. L. Sivco, C. Sirtori, A. L. Hutchinson, and A. Y. Cho, Science **264**, 553 (1994).
[2]Y. Bai, S. R. Darvish, S. Slivken, W. Zhang, A. Evans, J. Nguyen, and M. Razeghi, Appl. Phys. Lett. **92**, 101105 (2008).
[3]P. Q. Liu, A. J. Hoffman, M. D. Escarra, K. J. Franz, J. B. Khurgin, Y. Dikmelik, X. Wang, J.-Y. Fan, and C. F. Gmachl, Nat. Photonics **4**, 95 (2010).
[4]Y. Bai, S. Slivken, S. Kuboya, S. R. Darvish, and M. Razeghi, Nat. Photonics **4**, 99 (2010).
[5]J. Faist, C. Gmachl, F. Capasso, C. Sirtori, D. L. Sivco, J. N. Baillargeon, and A. Y. Cho, Appl. Phys. Lett. **70**, 2670 (1997).
[6]C. Gmachl, D. L. Sivco, J. N. Baillargeon, A. L. Hutchinson, F. Capasso, and A. Y. Cho, Appl. Phys. Lett. **79**, 572 (2001).
[7]A. Wittmann, A. Hugi, E. Gini, N. Hoyler, and J. Faist, IEEE J. Quantum Electron. **44**, 1083 (2008).
[8]A. Kosterev, G. Wysocki, Y. Bakhirkin, S. So, R. Lewicki, M. Fraser, F. Tittel, and R. Curl, Appl. Phys. B **90**, 165 (2008).
[9]M. Brandstetter, L. Volgger, A. Genner, C. Jungbauer, and B. Lendl, Appl. Phys. B **110**, 233 (2013).
[10]A. Kosterev and F. Tittel, IEEE J. Quantum Electron. **38**, 582 (2002).
[11]P. Patimisco, G. Scamarcio, F. Tittel, and V. Spagnolo, Sensors **14**, 6165 (2014).
[12]B. Mizaikoff, Chem. Soc. Rev. **42**, 8683 (2013).
[13]Y.-C. Chang, P. Wägli, V. Paeder, A. Homsy, L. Hvozdara, P. van der Wal, J. D. Francesco, N. F. de Rooij, and H. P. Herzig, Lab Chip **12**, 3020 (2012).
[14]M. Sieger, F. Balluff, X. Wang, S.-S. Kim, L. Leidner, G. Gauglitz, and B. Mizaikoff, Anal. Chem. **85**, 3050 (2013).
[15]R. Shankar, I. Bulu, and M. Lončar, Appl. Phys. Lett. **102**, 051108 (2013).
[16]N. Fabricius, G. Gauglitz, and J. Ingenhoff, Sens. Actuators, B **7**, 672 (1992).
[17]L. Gendron, M. Carras, A. Huynh, V. Ortiz, C. Koeniguer, and V. Berger, Appl. Phys. Lett. **85**, 2824 (2004).
[18]M. Graf, N. Hoyler, M. Giovannini, J. Faist, and D. Hofstetter, Appl. Phys. Lett. **88**, 241118 (2006).
[19]H. Schneider, C. Schonbein, M. Walther, K. Schwarz, J. Fleissner, and P. Koidl, Appl. Phys. Lett. **71**, 246 (1997).
[20]D. Hofstetter, M. Beck, and J. Faist, Appl. Phys. Lett. **81**, 2683 (2002).
[21]B. Schwarz, P. Reininger, H. Detz, T. Zederbauer, A. M. Andrews, S. Kalchmair, W. Schrenk, O. Baumgartner, H. Kosina, and G. Strasser, Appl. Phys. Lett. **101**, 191109 (2012).
[22]B. Schwarz, P. Reininger, D. Ristanić, H. Detz, A. M. Andrews, W. Schrenk, and G. Strasser, Nat. Commun. **5**, 4085 (2014).
[23]D. Ristanic, B. Schwarz, P. Reininger, H. Detz, T. Zederbauer, A. M. Andrews, W. Schrenk, and G. Strasser, Appl. Phys. Lett. **106**, 041101 (2015).
[24]Y. Zou, K. Vijayraghavan, P. Wray, S. Chakravarty, M. A. Belkin, and R. T. Chen, in Conference on Lasers and Electro-Optics (CLEO), San Jose, CA, USA, 2015.
[25]O. Baumgartner, Z. Stanojevic, and H. Kosina, in *Monte Carlo Methods and Applications*, edited by K. K. Sabelfeld and I. Dimov (De Gruyter Borovets, Bulgaria, 2012), Vol. 59, p. 67.
[26]P. Reininger, B. Schwarz, H. Detz, D. MacFarland, T. Zederbauer, A. M. Andrews, W. Schrenk, O. Baumgartner, H. Kosina, and G. Strasser, Appl. Phys. Lett. **105**, 091108 (2014).
[27]M. Beck, J. Faist, U. Oesterle, M. Ilegems, E. Gini, and H. Melchior, IEEE Photonics Technol. Lett. **12**, 1450 (2000).
[28]A. Delga, L. Doyennette, M. Carras, V. Trinité, and P. Bois, Appl. Phys. Lett. **102**, 163507 (2013).